An Ultra-Compact Common-Mode Bandstop Filter With Modified-T Circuits in Integrated Passive Device (IPD) Process

Chih-Ying Hsiao, *Student Member, IEEE*, Yang-Chih Huang, *Student Member, IEEE*, and Tzong-Lin Wu, *Fellow, IEEE*

***Abstract*—Based on multi-cell modified-T circuits, this paper proposes a novel circuit topology to realize a common-mode bandstop filter with differential-mode all-pass characteristics for high-speed digital differential circuits. The circuit behaviors for both differential and common modes are analyzed based on symmetrical network analysis techniques. Two transmission zeros at common mode can be synthesized by the derived formulas. The proposed design flow is used to realize a test sample in the integrated passive device process. Simulated and measured results are in good agreement. The common-mode suppression band ($|S_{cc21}| < -10$ dB) is from 1.6 to 4.7 GHz, whose fractional bandwidth is nearly 100%. The cutoff frequency of the differential mode can maintain up to 10 GHz with a constant group delay. Moreover, eye diagrams under different signaling rates all perform well. Compared with the other literature, the proposed common-mode filter has a very wide common-mode stopband, the highest differential-mode cutoff frequency up to 10 GHz, and the most compact circuit size of $0.017\ \lambda_g \times 0.016\ \lambda_g$.**

***Index Terms*—Common-mode filter (CMF), differential signaling, electromagnetic interference (EMI), integrated passive device (IPD).**

I. Introduction

SINCE differential signaling possesses high immunity to the external noise and the low-signal degradation from a non-ideal signal return path, this technique has been widely utilized in high-speed circuit designs [1], [2]. Those circuits designed by differential topology have two symmetrical signal conductors and a reference one. Such a three-conductor transmission system naturally has two fundamental propagating modes, i.e., differential mode and common mode [3]. The benefits mentioned above are only tenable when the signals are in pure differential mode. However, there are a lot of asymmetrical factors in real-world designs, such as bends in the routings, asymmetrical signal return path, unbalanced voltage swing, or the difference between the rising and falling time. Any of them produce mode conversion and then transform part of the differential-mode signals to common-mode noise. Common-mode noise is usually a dominant source to cause unintended radiation at discontinuous input/output (I/O) interfaces [4]. Thus, using a common-mode filter (CMF) to alleviate electromagnetic interference (EMI) or RF interference (RFI) becomes a crucial technique for optimizing the performance of high-speed differential systems.

There are three main challenges in designing a CMF for high-speed digital differential channel such as PCI-E, USB 3.0, HDMI, etc., which are: 1) broadband common-mode suppression; 2) all-pass characteristic with constant group delay for differential mode; and 3) a compact size with low cost. It is not easy to design a CMF that could achieve such three criteria simultaneously [2].

Conventionally, winding differential wires around the ferrite core is the commercial solution for blocking common-mode noise, but the frequency-dependent permeability of the ferrite core degrades its performances above gigahertz [5]. Not only the common-mode filtering band, but also the differential-mode cutoff frequency is limited below gigahertz. To further boost the performances, thin-film process with the ferrite material is employed. By this advanced technology, the cutoff frequency is modified and the size is also reduced. However, it needs advanced ferrite material with higher cost. Recently, a new common-mode filtering circuit without using a ferrite core was proposed to embed in packaging substrates [6], and several relative works [7]–[10] are followed to improve the performance. Coupled patterned ground structures (PGSs) are employed to extend the suppression bandwidth [7]. In [8] and [9], the complimentary split-ring resonator (CSRR) and mushroom-like structure are, respectively, put periodically beneath the differential pair to create a deep electromagnetic bandgap for the common mode (up to 30 dB). However, the circuit size is not small due to the periodic structures. Instead, a single unit with meandering signal lines is proposed to reduce the filter size at the cost of the weaker suppression level (about 10 dB) [10]. It has the most compact electrical size at that time and keeps a wide stopband (1.65–5.2 GHz) in the common mode, but its physical size (5-mm square) is still not small enough to apply in highly integrated packages or printed circuit boards (PCBs).

In this paper, combining the advantage of the integrated passive device (IPD) process for fabricating $R/L/C$ elements, a

Manuscript received February 04, 2015; revised June 25, 2015; accepted August 30, 2015. Date of publication October 05, 2015; date of current version November 03, 2015. This work was supported by the National Science Council, Taiwan, under Grant NSC 101-2221-E-002-127-MY3.

The authors are with the Department of Electrical Engineering and the Graduate Institute of Communication Engineering, National Taiwan University, Taipei 10617, Taiwan (e-mail: tlwu@ntu.edu.tw).

Color versions of one or more of the figures in this paper are available online at http://ieeexplore.ieee.org.

Digital Object Identifier 10.1109/TMTT.2015.2481412

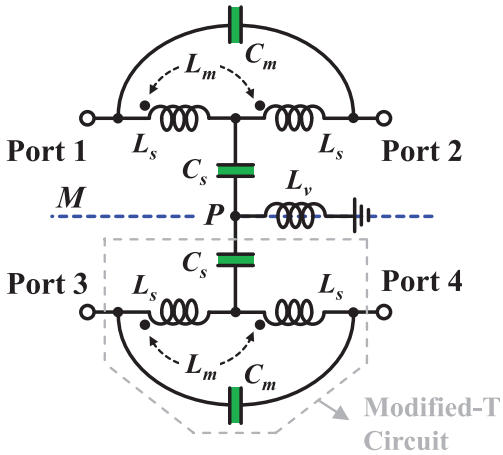

Fig. 1. Proposed new circuit topology for common-mode bandstop filter with modified-T circuits.

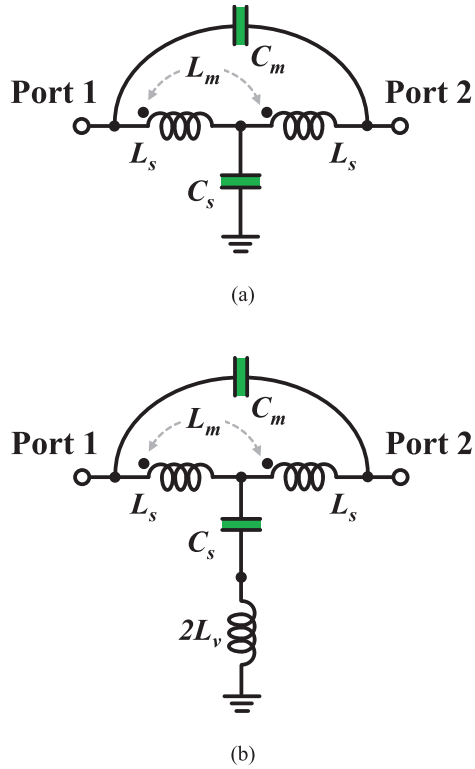

Fig. 2. Equivalent circuits of the proposed common-mode bandstop filter. (a) Odd mode. (b) Even mode.

novel circuit topology of modified-T circuits with a common inductor shorted to the ground is proposed to realize an ultra-compact CMF. This four-port network will become a two-port modified-T network with odd symmetry, and with even symmetry this network will become a two-port bandstop filter due to the contribution of the inductor shorted to the ground. Therefore, this circuit performs low insertion loss in the differential mode and broad stopband in the common mode. In addition, since a broadband and flat group delay is also critical to keep good signal integrity with a good eye diagram opening, a technique of a cascading multi-cell modified-T CMF is proposed to enhance the group-delay response. At the same time, a synthesizing flow as well as the corresponding formula is derived in this paper to offer a complete solution for common-mode noise suppression. To validate the proposed solution, a test circuit with a physical size of only 1×0.95 mm^2 or $0.017\ \lambda_g \times 0.016\ \lambda_g$ (λ_g is the wavelength with respect to the central frequency of the common-mode stopband) is demonstrated. The CMF has a good differential mode group delay under 10 GHz and can offer at least 10-dB common-mode noise suppression from 1.6 to 4.7 GHz, which is more than 100% of fractional bandwidth. Compared with those published in the literature, this work is the most compact CMF with the widest passband for differential signals.

II. Common-Mode Filter With Modified-T Circuits

A. Circuit Topology for Common-Mode Bandstop Filter

The proposed circuit topology for the common-mode bandstop filter is shown in Fig. 1. It is a four-port network with differential inputs at ports 1 and 3, and differential outputs at ports 2 and 4. Two parallel and identical modified-T circuits are between input and output ports. These two modified-T circuits are connected at node P and to the ground through an inductor (L_v). The modified-T circuit is a five-element network consisting of two series inductors (L_s), one shunt capacitor (C_s), one mutual inductance (L_m) between two L_s, and one mutual capacitance (C_m) between the input and output port. As shown in Fig. 1, there is a symmetrical line M crossing node P along the signal propagation direction. The circuits at two sides of the line M are identical. Due to the symmetrical property, an even- and odd-mode analysis technique can be applied to separate the proposed four-port network to the differential- and common-mode circuit individually by applying proper boundary conditions at the symmetrical line M.

B. Equivalent Circuit and Design for Differential Mode

At odd (or differential) mode excitation, node P becomes a virtual ground potential due to the perfect electrical wall at line M. The differential-mode circuit is just a modified-T circuit, as shown in Fig. 2(a), which has been well discussed in the past literature [11].

Originally, a modified-T circuit was used as an impedance transformer in integrated circuit (IC) designs [12], [13]. Recently, it was proven the modified-T circuit can exactly emulate the behavior of a lossless transmission line with the characteristic impedance (Z_0) and the propagating delay $(\tau = \theta/\omega)$, where θ is the electrical length of the transmission line. The equivalent relation between the modified-T circuit and a segment of lossless transmission line has been derived in [11]. They are repeated as follows for convenience:

$$L_s = Z_0\tau\left(0.25 + \frac{1}{\pi^2}\right) \tag{1a}$$

$$C_s = \frac{\tau}{Z_0} \tag{1b}$$

$$L_m = Z_0\tau\left(0.25 - \frac{1}{\pi^2}\right) \tag{1c}$$

$$C_m = \frac{\tau}{(Z_0 \cdot \pi^2)}. \tag{1d}$$

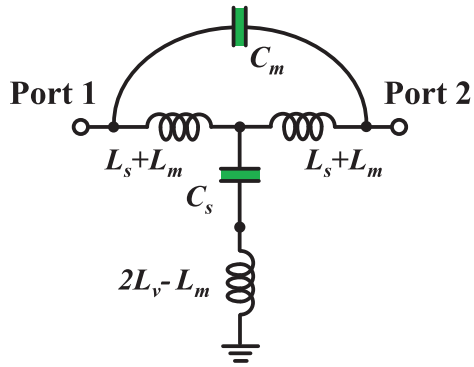

Fig. 3. Symmetrical even-mode equivalent circuit.

Based on this equivalence, it is obvious the modified-T circuit can be seen as an all-pass circuit if two ports are matched to Z_0.

C. Equivalent Circuit and Transmission Zeros for Common Mode

On the other hand, node P will be open circuit while ports 1 and 3 (or ports 2 and 4) are excited by in-phase signals, i.e., common mode. The equivalent circuit is depicted in Fig. 2(b), which is a two-port network composed of a modified-T circuit shorted to ground through an inductor $(2L_v)$. Due to this inductor, the two-port network behaves as a bandstop filter with two transmission zeros. In the following, the relationships between the transmission zeros and the corresponding values of the lumped L/C elements will be derived.

Using network transformation, the circuit shown in Fig. 2(b) is equivalent to the circuit shown in Fig. 3. It is obvious that this circuit is a symmetrical circuit between two ports. Based on the theory of symmetrical network analysis [14], the transmission coefficient of the even-mode equivalent circuit can be expressed as

$$S_{21} = \frac{Z_S\left(Z_{\text{in,even}} - Z_{\text{in,odd}}\right)}{\left(Z_{\text{in,even}} + Z_S\right)\left(Z_{\text{in,odd}} + Z_S\right)} \tag{2}$$

where $Z_{\text{in,even}}$ and $Z_{\text{in,odd}}$ are input impedances seen into one of the two ports when they are excited symmetrically and anti- symmetrically, respectively. Z_S is denoted as the system impedance, typically 50 Ω. $Z_{\text{in,even}}$ and $Z_{\text{in,odd}}$ of the symmetrical even-mode equivalent circuit are derived as follows:

$$Z_{\text{in,even}} = \frac{2 - \omega^2 C_s(L_s - L_m + 4L_v)}{j\omega C_s} \tag{3a}$$

$$Z_{\text{in,odd}} = \frac{j\omega(L_s + L_m)}{1 - 2\omega^2(L_s + L_m)C_m}. \tag{3b}$$

According to (2), it is apparent that S_{21} of the even-mode equivalent circuit will be zero if

$$Z_{\text{in,even}} = Z_{\text{in,odd}}. \tag{4}$$

Substituting (3a) and (3b) into (4), a linear quartic equation of ω can thus be derived as

$$\begin{aligned}&\left[C_sC_m(L_s + L_m)(L_s - L_m + 4L_v)\right]\omega^4 \\ &\quad - \left[2C_m(L_s + L_m) + C_s(2L_v - L_m)\right]\omega^2 + 1 = 0.\end{aligned} \tag{5}$$

TABLE I
DESIGN EXAMPLE AND THEIR CORRESPONDING LUMPED-ELEMENT VALUES

GIVEN SPECIFICATION	LUMPED-ELEMENT VALUES CALCULATED BY THE GIVEN SPECIFICATION	
$f_1 =$ 2 GHz	$L_s = 1.8\ nH$	$C_s = 2.05\ pF$
$f_2 =$ 4 GHz	$L_m = 0.76\ nH$	$C_m = 0.207\ pF$
$2Z_0 =$ 100 Ω	$L_v = 2.06\ nH$	

The frequencies of two transmission zeros (ω_1, ω_2) can be obtained by solving (5) and expressed as

$$\omega_{1,2} = \sqrt{\frac{-B \pm \sqrt{B^2 - 4A}}{2A}} \tag{6}$$

where

$$\begin{aligned}A &= C_sC_m(L_s + L_m)(L_s - L_m + 4L_v) \\ B &= -\left[2C_m(L_s + L_m) + C_s(2L_v - L_m)\right]\end{aligned}$$

and $\omega_1 < \omega_2$.

From the derivation in (2)–(6), it has been proven that the proposed circuit topology can provide two transmission zeros at common-mode excitation if there are two positive real solutions in (6), or under the condition of $B^2 - 4A > 0$. Therefore, by appropriately designing L/C parameters of this circuit, one can achieve the desired common-mode performance through designing the transmission zeros.

D. Circuit Synthesis and Examples

As mentioned in Section II-C, (6) can estimate the transmission zeros (ω_1, ω_2) for the given lumped element values, (L_s, C_s, L_m, C_m) and L_v. However, from the design viewpoint, synthesizing those L/C values for given transmission zeros (ω_1, ω_2) is very helpful. For this purpose, substituting (1a)–(1d) to (6) for (ω_1, ω_2), the independent variables (L_v and τ) can be solved and represented as

$$L_v = \frac{Z_0}{2}\left(\frac{\pi^2}{\tau^3\omega_1^2\omega_2^2} - \frac{\tau}{\pi^2}\right) \tag{7}$$

$$\tau = \sqrt{\frac{(\omega_1{}^2 + \omega_2{}^2) - \sqrt{(\omega_1{}^2 - \omega_2{}^2)^2 + (\pi\omega_1\omega_2)^2}}{2\omega_1{}^2\omega_2{}^2\left(\frac{1}{\pi^2 - 0.25}\right)}}. \tag{8}$$

Next, a lossless example is used to verify the design formulas. Two transmission zeros of common mode are set at $f_1 = 2$ GHz and $f_2 = 4$ GHz and the characteristic impedance of differential mode $(2Z_0)$ is set as 90 Ω. First, the emulating propagating delay of the modified-T circuit (τ) is obtained from (8) with the known f_1 and f_2. Substituting τ and Z_0 into (1a)–(1d) and (7), (L_s, C_s, L_m, C_m) and L_v are then obtained. These parameters are listed in Table I. Transmission coefficients of the differential and common mode ($|S_{dd21}|$ and $|S_{cc21}|$) of this example are plotted in Fig. 4. As expected, the proposed circuit behaves like an all-pass filter in the differential mode from dc to 10 GHz ($|S_{dd21}| > -3$ dB) and a bandstop filter in the common mode

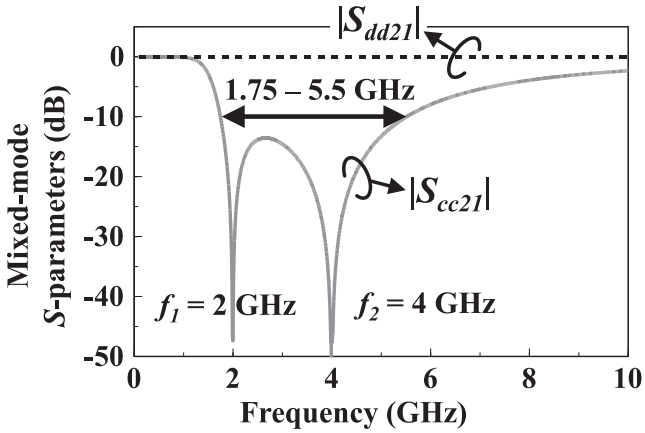

Fig. 4. Simulated results of the lossless example ($f_1 = 2$ GHz, $f_2 = 4$ GHz, and $2Z_0 = 100\ \Omega$).

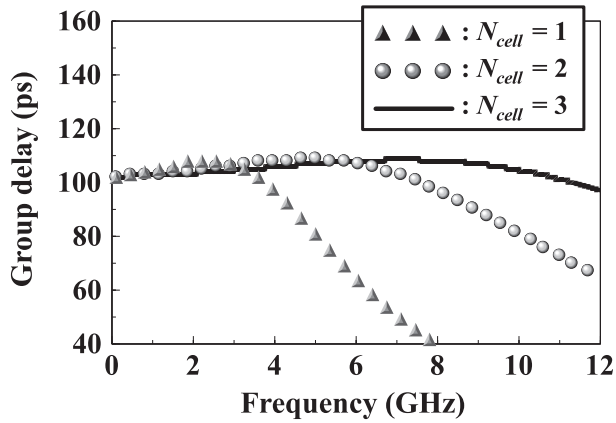

Fig. 5. Group delay with different cell numbers of the modified-T circuits.

from 1.75 to 5.5 GHz ($|S_{cc21}| < -10$ dB). Two transmission zeros are exactly located at 2 and 4 GHz. The group-delay response will be shown as the one-cell line of Fig. 5. The simulated results validate the correctness of the previously derived design formulas.

E. Group Delay With Multi-Cell Modified-T Circuits

For high-speed digital signaling, insertion loss of the filter is not the only factor to affect the signal integrity in the time domain. Flat group delay is another equally important factor to influence the signal quality. Since high-speed digital signals consist of very wideband frequency components, a linear phase or constant group delay for differential mode is an important property in CMF design. Fig. 5 shows the frequency response of the group delay of the previous design example ($N_{\text{cell}} = 1$). It is clearly seen that the group delay keeps flat (about 62 ps) with less than 10% variation only below 4 GHz, and it drops significantly to less than 40 ps at 10 GHz. This characteristic limits the application of this CMF on high-speed interfaces.

One way to solve this problem is using multi-cell modified-T circuits, as shown in Fig. 6. The L/C values of each sub modified-T circuit ($L_s{}', C_s{}', L_m{}', C_m{}'$) are obtained by equally dividing the corresponding L/C values of the original modified-T circuit by the cell number N_{cell} , i.e.,

$$(L_s{}', C_s{}', L_m{}', C_m{}') = \left(\frac{L_s}{N_{\text{cell}}}, \frac{C_s}{N_{\text{cell}}}, \frac{L_m}{N_{\text{cell}}}, \frac{C_m}{N_{\text{cell}}}\right). \quad (9)$$

It is noted that all sub modified-T circuits are connected to ground through the same inductor L_v at node P.

Fig. 5 also shows the frequency responses of the differential-mode group delays for different cell numbers, $N_{\text{cell}} = 2$ and 3.

It is seen that the bandwidth of flat group delay (variation <10%) can be extended to 8 and 12 GHz, respectively, for $N_{\text{cell}} = 2$ and 3. As can be seen, using multi-cell modified-T circuits is an effective way to extend the bandwidth of constant group delay. Besides, because L/C values are reduced through the multi-cell concept, the required circuit area will not be significantly increased even though N_{cell} is increased. To validate the improvement by using the multi-cell design, measured

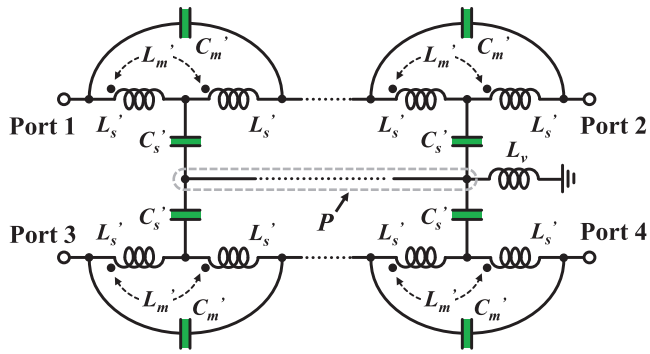

Fig. 6. Proposed common-mode bandstop filter topology with multi-cell modified-T circuits.

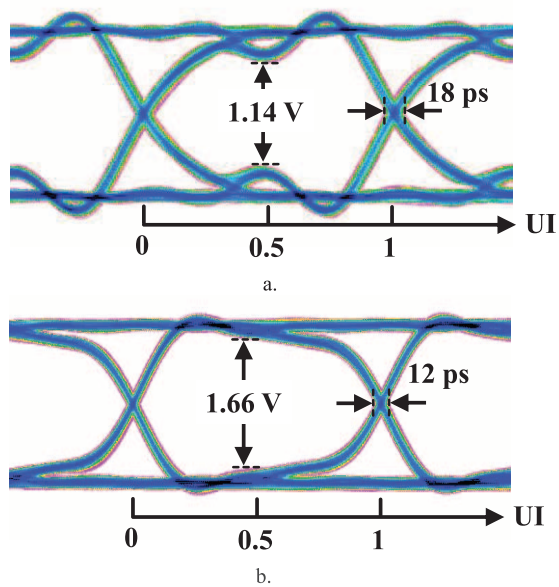

Fig. 7. Measured 5-Gb/s eye diagrams of: (a) one-cell case and (b) three-cell case.

5-Gb/s eye diagrams of one- and three-cell cases are also compared as shown in Fig. 7.

In practice, increasing the cells of modified-T circuit may also include extra material losses for differential signals, so a compromise between the cell number and the insertion losses should

be made. However, using multiple cells of a modified-T circuit is a simple and direct approach to enhance group delay and also compatible to the proposed design flow. In addition, as validated by measurement results, though the three-cell case introduces slightly higher insertion loss in the differential mode, the eye diagram of the three-cell case is still much better than that of the one-cell modified-T circuit, as shown in Fig. 7. The eye high is increased from 1.14 to 1.66 V and the jitter is reduced from 18 to 12 ps as the CMF is changed from one cell to three cells. These results show that the enhancement of group delay is critical for the eye diagram and therefore the benefit of reasonably increasing the cell number is obvious.

F. Design Flow of Proposed Common-Mode Bandstop Filter

The design flow of the proposed common-mode bandstop filter is itemized as follows.

Step 1) Assign the frequencies of two desired transmission zeros (ω_1, ω_2) for the common mode and the characteristic impedance Z_0.

Step 2) Obtain the emulating propagating delay τ by (8).

Step 3) Obtain (L_s, C_s, L_m, C_m) by (1a)–(1d) and L_v by (7) with the derived τ in Step 2.

Step 4) Decide the cell number N_{cell} according to the required group-delay bandwidth. Typically, two or three cells are good enough for practical applications.

Step 5) Obtain (L_s', C_s', L_m', C_m') by (9) with N_{cell} decided in Step 4.

Step 6) Optimization is essential after all elements are routed together.

III. Implementation and Measurement

A. Design and Fabrication

Following the design flow, a three-cell CMF $(N_{\text{cell}} = 3)$ is designed and realized with two desired common-mode transmission zeros at 2 and 4 GHz. The characteristic impedance of the differential mode is 100 Ω.

Firstly, the required propagation delay $\tau = 102$ ps is obtained by Step 2. Using Step 3, (L_s, C_s, L_m, C_m) and L_v are determined as (1.8 nH, 2.05 pF, 0.76 nH, 0.207 pF) and 2.06 nH, respectively. (L_s', C_s', L_m', C_m') are then obtained by dividing (L_s, C_s, L_m, C_m) by 3, and their values are (0.6 nH, 0.683 pF, 0.253 nH, 0.069 pF). Subsequently, this sample is realized by the IPD process [15], [16], which is attractive to fabricate $R/L/C$ elements due to the slight parasitic effect below 10 GHz. The IPD process utilized in this paper is constructed on a silicon substrate with 650-μm thickness, and the stackup is represented in Fig. 8. Above the silicon substrate, there are three metal layers (M1, M2, and M3) and two kinds of dielectrics [D1 and benzocyclobutene (BCB)]. The bottom metal layer, denoted as M1, is 1 μm thick and is mainly used as one electrode plate of metal–insulator–metal (MIM) capacitors. The middle metal layer, denoted as M2, is of 0.65-μm thickness. It is only used as the other electrode-plate of MIM capacitors or just be the connecting pad to link M1 and M3. The dielectric (D1) clipped by M1 and M2 is only 0.2 μm thick with the high dielectric constant (ε_r) of 6.7. As a result,

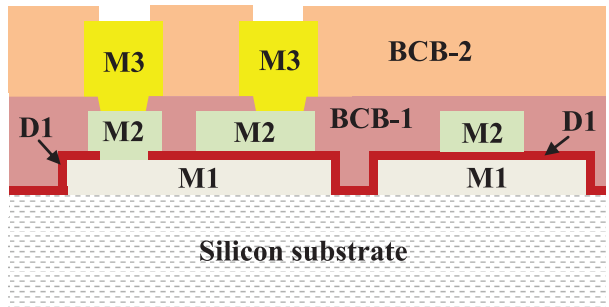

Fig. 8. Stackup of the utilized IPD process on silicon substrate.

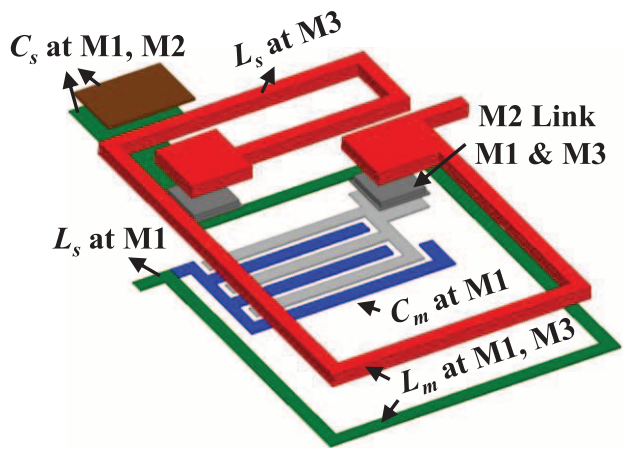

Fig. 9. 3-D view of the unit cell of modified-T circuit in the stack-up of IPD process.

M1 and M2 have a benefit to provide a large capacitance in a small space and the minimum capacitance is about 0.5 pF. Next, the top metal layer (M3) has the thickness of 10 μm and its main function is to make inductor coils with a high quality factor. The dielectric covering M2 and M3 is called BCB and the dielectric constant is 2.65.

In order to get the unit cell of the modified-T circuit with accurate values, each element is extracted separately with the help of a commercial full-wave simulator (HFSS). As we have known, a mutual term (L_m') is required to be induced by two series inductors (L_s'). Hence, as shown in Fig. 9, two L_s' are put projective to each other for forming a larger mutual term. One of them is routed at M1 and the other is put at M3. C_s' is then made by the MIM capacitor between M1 and M2, while C_m' is realized by the interdigital capacitor because it is just 0.069 pF, which is much smaller than the minimum available capacitance of the MIM capacitor. The 3-D view of the unit cell of the modified-T circuit is displayed in Fig. 9. Next, L_v is suggested to be realized by two inductors in parallel in order to make the circuit layout fully symmetric. Finally, when all elements are arranged together, some fine tunes are required because the interaction among them will change the original values.

Following the above procedures, the test sample is fabricated and displayed in Fig. 10. As shown in this figure, the real area that this test sample occupied is 1×0.95 mm^2. The remaining parts are the surrounding ground and the probing pads for measurement.

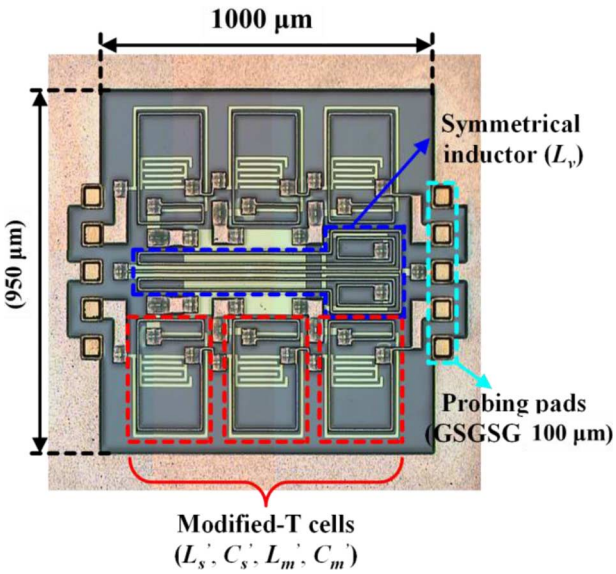

Fig. 10. Top view of the fabricated test sample. The circuit dimension is 1×0.95 mm^2 without considering the surrounding ground and probing pads.

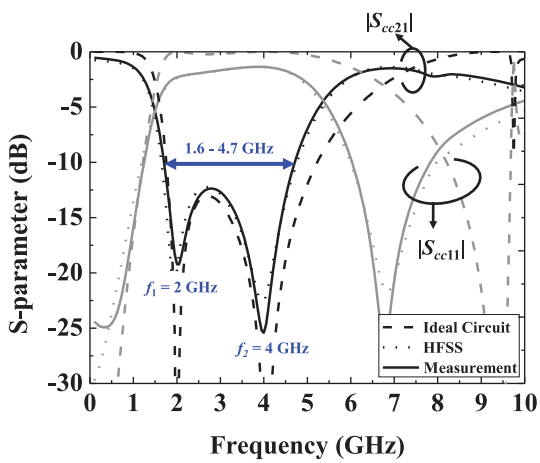

Fig. 11. Simulated and measured common-mode responses.

B. Performances in Frequency Domain

Mixed-mode S-parameters are employed to verify the circuit performances in the frequency domain. Our measurement is carried out by an Agilent four-port vector network analyzer (Agilent N5230A) with two 100-μm ground–signal–ground–signal–ground (GSGSG) probes. The frequency responses of transmission and reflection coefficient at common mode ($|S_{cc21}|$ and $|S_{cc11}|$) are shown in Fig. 11. The solid lines are the full-wave simulated results calculated by HFSS, and the dash lines are measured ones. It is obvious that $|S_{cc21}|$ of both simulated and measured results meet the desired performance, two transmission zeros at 2 and 4 GHz. Moreover, the common-mode stopband as the rejection level is more than 10 dB is from 1.6 to 4.7 GHz. The fractional bandwidth is about 100%. As seen in Fig. 11, $|S_{cc11}|$ cannot approach to 0 dB within the common-mode stopband because the common-mode energy is dissipated by the silicon substrate.

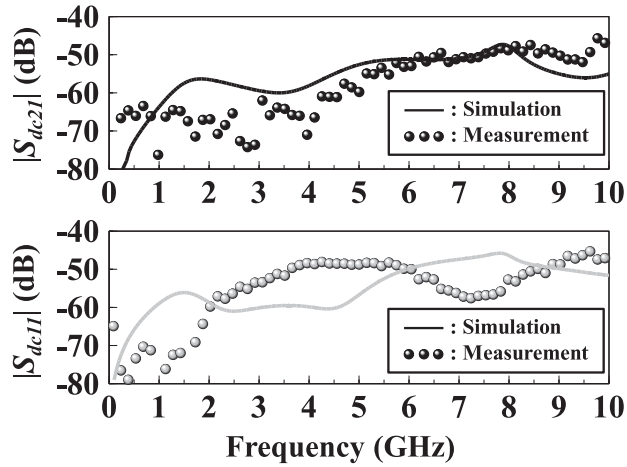

Fig. 12. Simulated and measured mode conversion level.

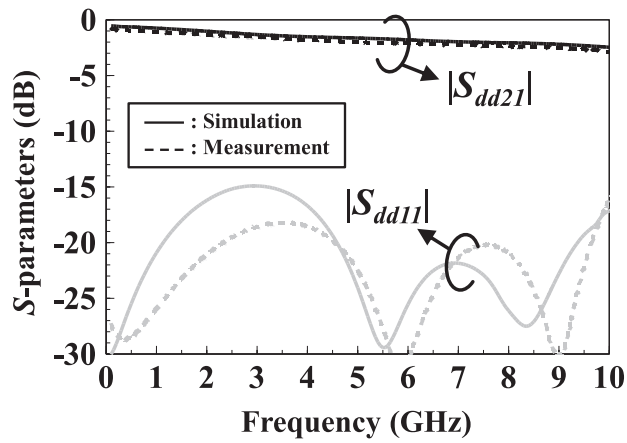

Fig. 13. Simulated and measured differential-mode responses.

Fig. 12 displays the simulated and measured mode conversion level ($|S_{dc21}|$ and $|S_{dc11}|$), which is all less than -45 dB below 10 GHz. The mode conversion of this test sample is very small due to the symmetrical layout.

Besides good common-mode suppression performance, another important criterion in designing a CMF is low insertion loss with constant group delay for differential mode from dc to very high frequency. Fig. 13 exhibits the differential-mode responses of the transmission and reflection coefficient, $|S_{dd21}|$ and $|S_{dd11}|$, both by measurement and simulation. The agreement between them is good. As can be seen, $|S_{dd11}|$ is less than -15 dB below 10 GHz, which discloses that the test sample is of a good matching condition to the terminal impedance. The 3-dB cutoff frequency of the differential-mode insertion loss $|S_{dd21}|$ is about 10 GHz by measurement. The insertion loss is mainly caused by the energy dissipation in the silicon substrate.

Furthermore, the group delay of the differential mode is also measured and simulated in Fig. 14. It can be seen that its variation from dc to 10 GHz is small and less than 30 ps. The constant group delay avoids the dispersion of the high-speed differential signals, and will keep the eye diagram (or signal integrity) in a good quality when the signals pass through this circuit. This

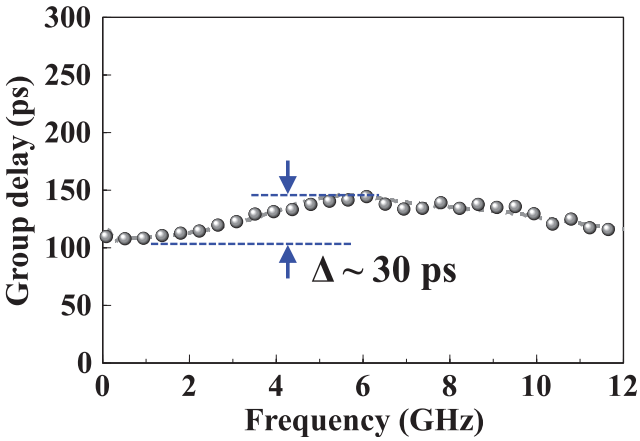

Fig. 14. Simulated and measured group delay of differential mode.

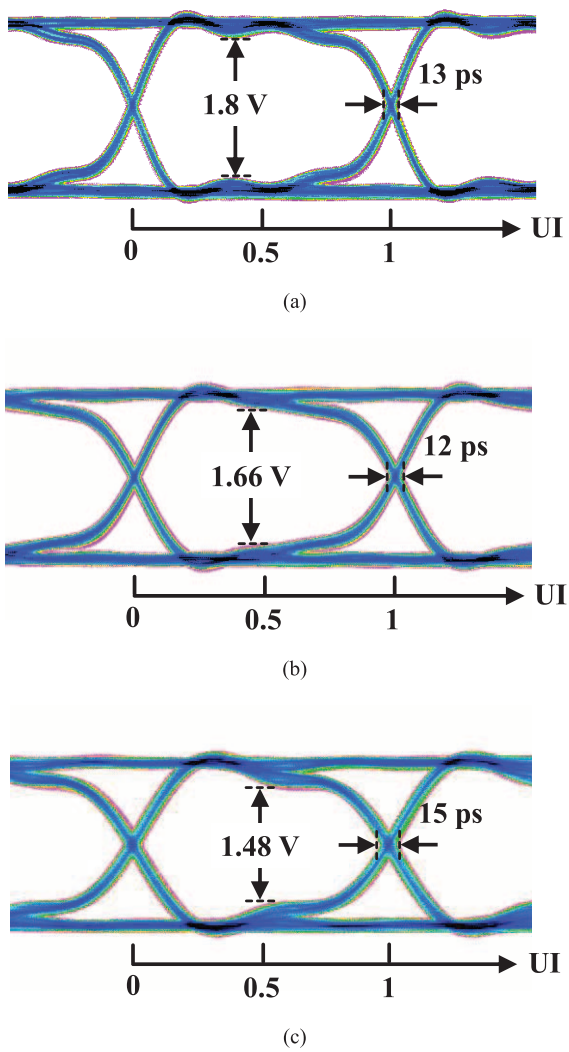

Fig. 15. Measured eye diagrams with different data rates. (a) 4 Gb/s. (b) 5 Gb/s. (c) 6 Gb/s.

result demonstrates that using multi-cell modified-T circuits indeed improve the dispersive problem.

C. Performances in Time Domain

An eye diagram in the time domain is an intuitive method to estimate how a circuit influences the signal quality of the differential signals in a pseudorandom bit sequence (PRBS). It simultaneously relates to the magnitude and phase information of S_{dd21} in the frequency domain from dc to very high frequency. In the eye diagram, eye height and jitter are two major metrics used to evaluate the signal quality. The larger the values they are, the better the signal quality the circuits can keep.

In our time-domain experiment, a pattern generator launches 2-V PRBS differential signals into the test sample, and the waveform is then captured at the output ports by a digital oscilloscope. Fig. 15 shows eye diagrams of 4, 5, and 6 Gb/s. The corresponding information of the eye height and jitter are marked on each figure. It can be found that all the opening of the eye patterns keep in a good situation under different data rates. The variation in jittering is within 2–3 ps and the maximum eye height variation is 0.32 V. They are acceptable for digital circuit designers. Such results prove again that using three-cell modified-T circuits is helpful to enhance the differential-mode bandwidth of the CMF and maintain a good signal quality for high-speed signaling rates.

TABLE II
COMPARISON COMMON-MODE FILTERS

	Process /Layer	Circuit Area (λ_g^2)	Stopband of CM (GHz)	Bandwidth of DM (GHz)	FBW < -10 dB
[6]	PCB/2	0.5618	3.1 – 6.9	7	76%
[7]	PCB/2	0.2304	3.6 – 10	8.4	94%
[8]	PCB/2	0.0602	1.1 – 2.1	---	54%
[9]	LTCC	0.0228	3.8 – 7.1	7.6	60%
[10]	PCB	0.0121	1.65 – 5.2	8.0	104%
This Work	IPD	0.0003	1.6 – 4.7	10	100%

• FBW stands for the fractional bandwidth, which is calculated by $2(\omega_2 - \omega_1)/(\omega_2 + \omega_1)$ where ω_1 and ω_2 are the angular frequencies of lower and higher bound of common-mode stopband, respectively.
• PCB stands for printed circuit board, and the dielectric is FR4 epoxy. LTCC stands for low-temperature co-fired ceramic.

Table II shows the performance comparison among this work and several previous common-mode bandstop filters. As can be observed, this work has the smallest physical and electrical sizes. It is worth noting that its electrical size is about 45 times smaller than the smallest one developed over the past few years. In addition, the cutoff frequency for the proposed filter can reach 10 GHz with the differential-mode insertion loss less than 3 dB, which is the widest one compared with others. The common-mode rejection bandwidth is also kept around 100%, wide enough for most of high-speed digital application.

IV. CONCLUSION

A novel topology based on multi-cell modified-T circuits are proposed to realize a common-mode bandstop filter with all-pass characteristics (or flat response) for the differential mode. Based on the network analysis technique, design formulas for circuit elements are deduced and thus applied to fabricate a test sample with three-cell modified-T circuits using the IPD process. Measured results show an excellent performance in both the frequency and time domains. Two desired common-mode transmission zeros are nearly located at 2 and 4 GHz, and the fractional bandwidth is about 100% when $|S_{cc21}| < -10$ dB. The cutoff frequency of the differential mode is from

dc to 10 GHz with a flat group-delay response. Hence, an eye diagram in the time domain exhibits good eye opening up to 6 Gb/s. This design achieves an ultra-compact size ($0.017\ \lambda_g \times 0.016\ \lambda_g$) with the widest passband for the differential mode compared with previous works.

REFERENCES

[1] S. H. Hall and H. L. Heck, *Advanced Signal Integrity for High-Speed Digital System Design*. Hoboken, NJ, USA: Wiley, 2009.

[2] T.-L. Wu, F. Buesink, and F. Canavero, "Overview of signal integrity and EMC design technologies on PCB: Fundamentals and latest progress," *IEEE Trans. Electromagn. Compat.*, vol. 55, no. 4, pp. 624–638, Aug. 2013.

[3] C. Paul, *Analysis of Multiconductor Transmission Lines*, 2nd ed. Hoboken, NJ, USA: Wiley, 2008.

[4] B. Archambeault, S. Connor, and J. Diepenbrock, "EMI emissions from mismatch in high-speed differential signal trace and cables," in *Proc. IEEE Int. Electromagn. Compat. Symp.*, Honolulu, HI, USA, Jul. 2007, pp. 1–6.

[5] K. Yanagisawa, F. Zhang, T. Sato, K. Yanagisawa, and Y. Miura, "A new wideband common-mode noise filter consisting of Mn–Zn ferrite core and copper/polyimide tape wound coil," *IEEE Trans. Magn.*, vol. 41, no. 10, pp. 3571–3573, Oct. 2005.

[6] W.-T. Liu, C.-H. Tsai, T.-W. Han, and T.-L. Wu, "An embedded common mode suppression filter for GHz differential signals using periodic defected ground plane," *IEEE Microw. Wireless Compon. Lett.*, vol. 18, no. 4, pp. 248–250, Apr. 2008.

[7] S.-J. Wu, C.-H. Tsai, and T.-L. Wu, "A novel wideband common-mode suppression filter for GHz differential signals using coupled patterned ground structure," *IEEE Trans. Microw. Theory Techn.*, vol. 57, no. 4, pp. 848–855, Apr. 2009.

[8] J. Naqui *et al.*, "Split rings-based differential transmission lines with common-mode suppression," in *IEEE MTT-S Int. Microw. Symp. Dig.*, Baltimore, MD, USA, Jun. 2011.

[9] C.-H. Tsai and T.-L. Wu, "A broadband and miniaturized common-mode filter for gigahertz differential signals based on negative permittivity metamaterials," *IEEE Trans. Microw. Theory Techn.*, vol. 58, no. 1, pp. 195–202, Jan. 2010.

[10] C.-Y. Hsiao, C.-H. Tsai, C.-N. Chiu, and T.-L. Wu, "Radiation suppression for cable-attached packages utilizing a compact embedded common-mode filter," *IEEE Trans. Compon., Packag., Manuf. Technol.*, vol. 2, no. 10, pp. 1696–1703, Oct. 2012.

[11] T.-S. Horng, J.-M. Wu, L.-Q. Yang, and S.-T. Fang, "A novel modified-T equivalent circuit for modeling LTCC embedded inductors with a large bandwidth," in *IEEE MTT-S Int. Microw. Symp. Dig.*, 2003, pp. 1015–1018.

[12] L. Selmi, D. B. Estreich, and B. Ricci, "Small-signal MMIC amplifiers with bridged T-coil matching networks," *IEEE J. Solid-State Circuits*, vol. 21, no. 7, pp. 1093–1096, Jul. 1992.

[13] J. Paramesh and D. J. Allstot, "Analysis of the bridged T-coil circuit using the extra-element theorem," *IEEE Trans. Circuits Syst. II, Exp. Briefs*, vol. 53, no. 12, pp. 1408–1412, Dec. 2006.

[14] J. S. Hong and M. J. Lancaster, *Microstrip Filters for RF/Microwave Application*. New York, NY, USA: Wiley, 2001.

[15] Y.-S. Lin and J.-H. Lee, "Miniature ultra-wideband power divider using bridged T-coils," *IEEE Microw. Wireless Compon. Lett.*, vol. 22, no. 8, pp. 391–393, Aug. 2012.

[16] C.-H. Huang, T.-S. Horng, C.-C. Wang, C.-T. Chiu, and C.-P. Hung, "Optimum design of transformer-type Marchand balun using scalable integrated passive device technology," *IEEE Trans. Compon., Packag., Manuf. Technol.*, vol. 2, no. 8, pp. 1370–1377, Aug. 2012.

Chih-Ying Hsiao (S'07) received the B.S degree in communication engineering from Yuan-Ze University, Taoyuan, Taiwan, in 2009, and is currently working toward the Ph.D. degree at the Graduate Institute of Communication Engineering, National Taiwan University, Taipei, Taiwan.

His research interests include the design of maintaining signal integrity and reducing electromagnetic interference (EMI) problems of high-speed I/O circuits.

Yang-Chih Huang (S'14) received the B.S. degree in communication engineering from National Taiwan University, Taipei, Taiwan, in 2010, and is currently working toward the Ph.D. degree at the Graduate Institute of Communication Engineering, National Taiwan University.

His research interests include the design of maintaining signal integrity and the design of microwave elements.

Tzong-Lin Wu (S'93–M'98–SM'04–F'13) received the B.S.E.E. and Ph.D. degrees from National Taiwan University (NTU), Taipei, Taiwan, in 1991 and 1995, respectively.

From 1995 to 1996, he was a Senior Engineer with the Microelectronics Technology Inc., Hsinchu, Taiwan. From 1996 to 1998, he was with the Central Research Institute, Tatung Company, Taipei, Taiwan, where he was involved with the analysis and measurement of electromagnetic compatibility (EMC)/electromagnetic interference (EMI) problems of high-speed digital systems. From 1998 to 2005, he was with the Electrical Engineering Department, National Sun Yat-Sen University. He is currently a Distinguished Professor with the Department of Electrical Engineering, NTU, and serves as a Director with the Graduate Institute of Communication Engineering, NTU. In Summer 2008, he was a Visiting Professor with the Electrical Engineering Department, University of California at Los Angeles (UCLA). His research interests include EMC/EMI, signal/power integrity design for high-speed digital/optical systems, and microwave circuits.

Dr. Wu was the chair of the Taipei Section, Institute of Electronics, Information and Communication Engineer (IEICE) (2007–2011). He was the treasurer of the IEEE Taipei Section (2007–2008). He was a member of the Directors of the IEEE Taipei Section (2009–2010 and 2013–2014). He was a Distinguished Lecturer of the IEEE Electromagnetic Compatibility (EMC) Society (2008–2009). He was the co-chair of the 2007 IEEE EDAPS Workshop, the Technical Program Committee (TPC) chair of IEEE EDAPS Symposium (2010 and 2012), and general chair of the Asia–Pacific EMC Symposium (APEMC'15). He is an associate editor of the IEEE TRANSACTIONS ON ELECTROMAGNETIC COMPATIBILITY and the IEEE TRANSACTIONS ON COMPONENTS, PACKAGING, AND MANUFACTURING TECHNOLOGIES. He was the recipient of the Excellent Research Award and Excellent Advisor Award of NSYSU (2000 and 2003), the Wu Ta-You Memorial Award of the National Science Council (NSC) (2005), the Technical Achievement Award of the IEEE EMC Society (2009), the 2010 Best Paper Award of the IEEE TRANSACTIONS ON ADVANCED PACKAGING, and the Outstanding Research Award from NSC (2010 and 2013).